



HAL
open science

Morphological traits, niche-environment interaction and temporal changes in diatoms

Loïck Kléparski, Grégory Beaugrand, Martin Edwards, François Schmitt, Richard Kirby, Elsa Breton, François Gevaert, Emeline Maniez

► **To cite this version:**

Loïck Kléparski, Grégory Beaugrand, Martin Edwards, François Schmitt, Richard Kirby, et al.. Morphological traits, niche-environment interaction and temporal changes in diatoms. *Progress in Oceanography*, 2022, 201, pp.102747. 10.1016/j.pocean.2022.102747 . hal-04288026

HAL Id: hal-04288026

<https://normandie-univ.hal.science/hal-04288026v1>

Submitted on 15 Nov 2023

HAL is a multi-disciplinary open access archive for the deposit and dissemination of scientific research documents, whether they are published or not. The documents may come from teaching and research institutions in France or abroad, or from public or private research centers.

L'archive ouverte pluridisciplinaire **HAL**, est destinée au dépôt et à la diffusion de documents scientifiques de niveau recherche, publiés ou non, émanant des établissements d'enseignement et de recherche français ou étrangers, des laboratoires publics ou privés.

Morphological traits, niche-environment interaction and temporal changes in diatoms

Loïck Kléparski ^{1,2*}, Grégory Beaugrand ^{1*}, Martin Edwards ^{3,4}

François G. Schmitt ¹, Richard R. Kirby ⁵, Elsa Breton ¹, François Gevaert ¹, Emeline Maniez ¹

¹ Univ. Littoral Côte d'Opale, CNRS, Univ. Lille, UMR 8187 - LOG - Laboratoire d'Océanologie et de Géosciences, F-62930 Wimereux, France

² Marine Biological Association, Citadel Hill, Plymouth PL1 2PB, United Kingdom.

³ Plymouth Marine Laboratory, Prospect Place, Plymouth, PL13DH, United Kingdom.

⁴ University of Plymouth, School of Biological and Marine Sciences, Drake Circus, Plymouth, United Kingdom.

⁵ The Secchi Disk Foundation, Kiln Cottage, Gnaton, Yealmpton, PL8 2HU, United Kingdom.

* corresponding authors: loick.kleparski@hotmail.fr

Authors' contributions: L.K and G.B designed the study. L.K, G.B and E.M performed the analyses. L.K and G.B wrote the first draft and L.K, G.B, M.E, F.S, R.K, E.B, F.G and E.M discussed the results.

Competing interests: The authors declare no competing interests.

Keywords: annual diatom succession, cell elongation, ecological niche, morphological traits, phenology, North Sea, CPR survey.

26 **Abstract**

27 Annual phytoplankton succession is a key ecological phenomenon that drives marine species' life
28 cycles and energy flows within marine ecosystems. Identifying processes that control annual
29 succession is critical to anticipate climate-induced environmental perturbations of this phenomenon
30 and the consequences upon ecosystem functioning. Here, we demonstrate that diatoms in the North
31 Sea undergo strong morphological changes throughout the year and that species with similar
32 phenology possess comparable morphological traits (e.g. cell elongation) and ecological niches. The
33 spring and autumn periods appear to be dominated by oblates (flattened cells) whereas the summer
34 period is dominated by prolate (elongated cells). Elongation of the cell shape enhances buoyancy and
35 confers a selective advantage in stratified low-nutrient waters typical of summer without changing a
36 diatoms' surface area/volume ratio or its ability to absorb nutrients. Diatom shape thus appears to
37 have evolved as a key adaptation to a specific environment and confers upon a species its specific
38 niche and phenology, and therefore its place in the sequence of annual succession. As a result, shape
39 influences temporal changes in the abundance of diatoms and their putative response to
40 environmental forcing. We suggest that biogeochemical and earth-system models should include
41 diatom cell shape as a parameter in order to improve model predictions and help our understanding
42 of the consequences of climate change on marine ecosystems.

43

44 **1. Introduction**

45 Diatoms are a major phytoplankton clade that have evolved during the Middle Triassic when sea
46 levels were rising and continental margins were flooding (Falkowski et al., 2004). Diatoms'
47 subsequent increase in diversity during the mid-Cenozoic Era strongly influenced the global carbon
48 cycle (Katz et al., 2005). Today, diatoms account for about 40% of total marine primary production
49 and almost 40% of total particulate organic carbon exported to the deep ocean annually (Jin et al.,
50 2006; Nelson et al., 1995; Tréguer et al., 2018). Annually, the abundance of diatoms rises and falls on

51 a seasonal basis following a predictable pattern named “Annual Diatom Succession” (called hereafter
52 ADS).

53

54 In the North Sea, ADS is characterised by the succession of various species throughout the year, with
55 species such as *Skeletonema costatum* and *Thalassiothrix longissima* dominating in spring, *Guinardia*
56 *striata* and *G. flaccida* in summer and *Poroboscia indica* and *Bidulphia alternans* in autumn

57 (Caracciolo et al., 2021). ADS therefore determines the pulses of energy that influence the dynamics
58 of the whole marine ecosystem, the life cycle of many zooplankton and fish being coupled with the
59 peaks in primary production or species dominance (Cushing, 1990; Platt et al., 2003). Recently,
60 anthropogenic climate change has begun to alter diatom phenology and biogeography, and this is
61 likely to have strong consequences on trophic interaction and ecosystem functioning (Chivers et al.,
62 2017; Edwards and Richardson, 2004).

63

64 To predict the future consequences of climate change on marine ecosystems, we need to i) better
65 understand how diatom communities naturally form and reorganise at multiple time-scales and ii) to
66 identify the key elements and processes that control phenology. Morphological traits (i.e. cell size
67 and shape) are known to play an important role in diatom succession because they influence
68 resource uptake, buoyancy and predation, which are all properties that may explain seasonal
69 changes in species dominance (Behrenfeld, 2010; Caracciolo et al., 2021; Karp-Boss and Boss, 2016;
70 Margalef, 1978; Naselli-Flores et al., 2021; Naselli-Flores and Barone, 2011). The niche of a species
71 (i.e. the set of environmental parameters that enable a species to grow, maintain and reproduce) is
72 also of paramount importance as it controls the range of environmental conditions that a species can
73 tolerate (Hutchinson, 1957). Here, we investigate the relationships between species’ morphological
74 traits (size and shape), ecological niches, and phenology with the aim of identifying the key elements
75 and processes responsible for ADS.

76

77 **2. Materials and Methods**

78 **2.1. Biological data**

79 We used abundance data of 45 diatom species/taxa commonly sampled by the Continuous Plankton
80 Recorder (CPR) survey in the North Sea (51°N, 60°N, -3°E, 9°E; Supplementary Figure S1) between
81 1958 and 2017 (Reid et al., 2003). This long-term plankton monitoring programme has collected
82 plankton on a monthly basis in the extratropical regions of the North Atlantic Ocean and its adjacent
83 seas since 1946. The sampling machine is a high-speed plankton recorder towed behind voluntary
84 merchant ships at a depth of approximately 7 m (Beaugrand et al., 2003; Reid et al., 2003) (see
85 Supplementary Text S1 for an overview of the CPR limitations and Supplementary Text S2 for CPR
86 data availability)(Beaugrand et al., 2003; Reid et al., 2003). Each value of abundance corresponds to a
87 number of cells per CPR sample, which corresponds on average to 3 m³ of seawater filtered (Jonas et
88 al., 2004). We calculated a daily climatology of the abundance of 45 diatoms sampled by the CPR
89 survey. To account for all CPR samples collected between 1958 and 2017, we based our climatology
90 on 366 days. We applied twice a 6-order simple moving average on the matrix (366 days x 45
91 species/taxa) and standardized the abundance data between 0 and 1 for each species, following the
92 procedure described in Caracciolo and colleagues (Caracciolo et al., 2021).

93

94 **2.2. Environmental data**

95 Supplementary Text S2 provides key references and internet sites for each environmental dataset we
96 used. Sea Surface Temperature (SST; °C) originated from the NOAA OI SST V2 high resolution dataset
97 provided by the Earth System Research Laboratory, Physical Science Division, Boulder Colorado, USA.
98 Mixed Layer Depth (MLD; m) was provided by the Copernicus Marine Environment Monitoring
99 service (CMEMS) and originated from the Global Ocean Physical Reanalysis product
100 (GLOBAL_REANALYSIS_PHY_001_030). We used the MLD as a proxy of turbulence level (the deeper
101 the MLD is, the more active the wind-induced turbulence is likely to be) and stratification (a lower

102 MLD is in general associated with a higher stratification, which prevents nutrients recycling to the
103 surface).

104

105 Phosphate, silicate and nitrate concentrations ($\text{mmol}\cdot\text{m}^{-3}$) were provided by the CMEMS and came
106 from the Global Ocean Biogeochemistry Hindcast (GLOBAL_REANALYSIS_BIO_001_029).

107 Photosynthetically Active Radiation (PAR; $\text{mole}/\text{m}^2/\text{day}$) was provided by Globcolour Hermes. PAR
108 was estimated from satellites data. Euphotic depth of sea water (m) was provided by the NASA
109 Goddard Space Flight Center, Ocean Ecology Laboratory, Ocean Biology Processing Group. Euphotic
110 depth was calculated with Lee algorithm. Bathymetry (m) was provided by the British Oceanographic
111 Data Centre (BODC). Distance to nearest coastlines (km) was provided by the Nasa's Ocean Biology
112 Processing Group, Goddard Space Flight Center.

113

114 We calculated a daily climatology for each environmental parameter in the North Sea (Figure 2b-h
115 and Supplementary Figures S1 and S2a-c), based on the time period 1997-2017. The climatology of
116 the euphotic depth of sea water was based on the time period 2002-2017. Here also, we based our
117 climatologies on 366 days to match the diatom climatologies. We assumed that the difference of
118 time periods between biological (1958-2017) and environmental (1997-2017) datasets did not alter
119 our conclusions because the seasonal changes observed here, are much more important than
120 decadal changes (see Figure 4). The use of the full time period for CPR data was important to have a
121 more reliable daily climatology and we know that daily variability is much higher than decadal
122 variability, an assumption that has been checked for copepod biodiversity assessed from the CPR
123 data (Beaugrand et al., 2003).

124

125 The kinematic viscosity (in $\text{m}^2\cdot\text{s}^{-1}$) was assessed from SST daily climatology using equations from
126 Pilson (Pilson, 2013) and assuming a salinity of 35 (i.e. mean salinity of the North Sea).

127

128 Data on monthly long-term changes in SST ($^{\circ}\text{C}$), mean surface downward short-wave radiation flux
129 ($\text{W}\cdot\text{m}^{-2}$), and northward and eastward wind components ($\text{m}\cdot\text{s}^{-1}$) originated from the ERA5 dataset.
130 This monthly gridded dataset, which covered the period 1958-2017, were provided by the
131 Copernicus climate change service. Data on mean surface downward short-wave radiation flux (solar
132 radiations) were used as a proxy of PAR.

133

134 **2.3. Morphological traits**

135 *2.3.1. Cell shape*

136 We gathered together information on the geometrical shape of each species from the Global
137 Diatoms Database (Leblanc et al., 2012). Six different shapes were distinguished: cylinder, cylinder +
138 2 half spheres, rectangular box, prism on an elliptic base, prism on a parallelogram base and prism on
139 a triangular base (Supplementary Table S1).

140

141 *2.3.2. Oblates and prolates*

142 We also retrieved information on minimum and maximum cell dimensions (diameter/height or
143 length/width/height depending upon cell shapes). For cylindrical cells, we defined height as the
144 dimension perpendicular to cell diameter. For other geometrical shapes, we first converted them to a
145 cylinder of equivalent size: we calculated the area of the slice perpendicular to cell height (as defined
146 in the database) and estimated the diameter of the equivalent disk (i.e. the disk of equivalent
147 surface). Based on these cell dimensions, we divided diatoms into three groups: (i) oblates (i.e.
148 minimum height < minimum diameter and maximum height < maximum diameter), (ii) prolates (i.e.
149 minimum height > minimum diameter and maximum height > maximum diameter) and (iii)
150 oblates/prolates for the remaining species/taxa, meaning that they can be both oblates and prolates
151 (Supplementary Table S2).

152

153 *2.3.3. Other morphological indices*

154 Based on mean cell height (h) and diameter (d) (Supplementary Table S2), we estimated the area (s),
155 the volume (v) and the area/volume ratio (sv^{-1}) of each species by assimilating their shape to a
156 cylinder:

$$158 \quad s_{cylinder} = \pi d \left(\frac{d}{2} + h \right) \quad [1]$$

$$160 \quad v_{cylinder} = \frac{\pi}{4} d^2 h \quad [2]$$

162 We assessed an index of cell morphology, which had the advantage to be dimensionless:

$$164 \quad \delta = msv^{-1} \quad [3]$$

166 with m the cell maximum linear dimension (i.e. the mean cell diameter or height for oblates and
167 prolates, respectively). δ describes cell attenuation (i.e. reduction of one of the dimensions of the
168 cell volume or cell flattening) and its departure from a sphere (Naselli-Flores et al., 2021).

170 We estimated the maximum area of light interception normalized by volume (β). For oblates, we
171 calculated the ratio between disk area and volume as follows:

$$173 \quad \beta_{oblates} = \frac{\pi \left(\frac{d}{2} \right)^2}{v} \quad [4]$$

175 For prolates, we calculated the ratio between rectangle area (projection of a cylinder on a surface)
176 and volume:

$$178 \quad \beta_{prolates} = \frac{dh}{v} \quad [5]$$

179

180 **2.4. Predation**

181 We used abundance data of 74 small (≤ 2 mm) and 196 large (> 2 mm) copepods species/taxa
182 collected by the CPR survey in the North Sea (Supplementary Figure S1). We summed the total
183 abundance for small/large copepods in each CPR sample between 1958-2017 and then calculated a
184 daily abundance climatology for small/large copepods. We therefore obtained two vectors of 366
185 days (one vector for small and another for large copepods) with the daily mean abundance for
186 small/large copepods. As above, we applied twice a simple 6-order moving average and standardized
187 the abundance data between 0 and 1 (Supplementary Figure S2c).

188

189 **2.5. Phylogenetical classification**

190 Information on the phylogenetical classification of the 45 diatoms (family, order, superorder,
191 subclasses) was retrieved from the WORld Register of Marine Species (WORMS)
192 (<http://www.marinespecies.org/index.php>). (Supplementary Figure S3 and Table S3).

193

194 **2.6. Analyses**

195 *2.6.1. Principal Component Analysis (PCA)*

196 We characterized Annual Diatom Succession (ADS) by applying a standardized PCA on a matrix of
197 daily abundance climatology (366 days) x diatom species (45 species) (Figure 1a). We examined the
198 first three axes (principal components and eigenvectors) of the PCA because a test based on a
199 broken-stick distribution (Legendre and Legendre, 1998) revealed that the first three axes of the PCA
200 were significant, i.e. they were above average eigenvalues calculated by the broken-stick model
201 (Supplementary Table S4). Seasonal changes in diatom abundance were examined by the first three
202 principal components (PCs) and relationships between species were investigated by using the first
203 three normalized eigenvectors, which represented the correlation of the 45 diatoms with the first
204 three PCs. We tested the relationships between the first three principal components and the daily

205 climatology for SST, euphotic depth, PAR, MLD, mean small/large copepods abundance, viscosity,
206 silicate, phosphate and nitrate concentration by means of a Spearman rank correlation coefficient.
207 The significance of the correlation coefficients was tested by applying a Montecarlo test with 100,000
208 simulations (Figure 3 and Supplementary Table S5).

209

210 *2.6.2. Clustering*

211 We applied a cluster analysis based on the first three normalized eigenvectors of the PCA. First, we
212 calculated a squared matrix of Euclidean distance using the first three eigenvectors. Then we applied
213 a Ward linkage algorithm (Legendre and Legendre, 1998). The resulting dendrogram was cut using a
214 threshold of Euclidean distance of 8; this threshold was chosen because it enabled the identification
215 of three species groups that closely matched the seasonal patterns exhibited by the first three PCs
216 (Figure 1a, 3 and Supplementary Figures S2d-f, S4 and S5).

217

218 *2.6.3. Relationships between phenology and morphological traits*

219 We examined the relationships between the species groups and morphological traits in the space
220 defined by the first three eigenvectors: (i) geometrical shapes (Figure 1b), (ii) oblates/prolates (Figure
221 1c), (iii) height-diameter difference (Figure 1d), (iv) area/volume ratio (Figure 1e), (v) δ (Figure 1f), (vi)
222 mean cell diameter (Supplementary Figure S6a) and (vii) mean cell height (Supplementary Figure
223 S6b).

224

225 We tested the differences in the mean of the morphological indices (height-diameter
226 (Supplementary Table S6), mean cell diameter (Supplementary Table S7), mean cell height
227 (Supplementary Table S8), area/volume ratio (Supplementary Table S9) and δ (Supplementary Table
228 S10)) among species groups by means of a Kruskal-Wallis test and post-hoc tests.

229

230 *2.6.4. Comparison between morphological traits based on cylindrical and spheroidal shapes*

231 In our analyses, we assimilated diatom shapes to cylinders. To test whether our conclusions were
232 affected by this assumption, we also compared our results with those obtained by assimilating
233 diatom shapes to spheroids. Based on mean cell height (h) and diameter (d) (Supplementary Table
234 S2), we re-estimated the area (s), the volume (v) and the area/volume ratio (sv^{-1}) of each species
235 by assimilating their shape to spheroids as follows:

236

$$237 \quad s_{spheroid} = \frac{\pi d}{2} \left(d + \frac{h^2}{\sqrt{h^2 - d^2}} \sin^{-1} \frac{\sqrt{h^2 - d^2}}{d} \right) \quad [6]$$

238

$$239 \quad v_{spheroid} = \frac{\pi}{6} d^2 h \quad [7]$$

240

241 We examined the relationships between morphological traits (area, volume, area/volume ratio and
242 δ) when cells were based on cylinders (see equations 1-3) and spheroids by means of Pearson
243 correlation coefficients (Supplementary Figure S7a-d).

244

245 We also investigated the relationships between species groups and morphological traits estimated
246 with spheroidal shape in the space defined by the first three eigenvectors using (i) area/volume ratio
247 and (ii) δ (Supplementary Figure S7e-h).

248

249 Finally, we tested the differences in the mean of the morphological indices among species groups,
250 based on spheroidal shapes for area/volume ratio (Supplementary Table S11) and δ (Supplementary
251 Table S12), by means of a Kruskal-Wallis test and post-hoc tests.

252

253 *2.6.5. Relationships between morphological indices and the environment*

254 We also examined the relationships between m and area/volume ratio (Figure 1g-h), PAR and β
255 (Supplementary Figure S8), MLD and δ (Supplementary Figure S9), kinematic viscosity and δ

256 (Supplementary Figure S10) and between copepod abundance and height-diameter difference
257 (Supplementary Figure S11).

258

259 We calculated the Spearman rank correlation coefficient between m and area/volume ratio (Figure
260 1g), PAR and β (Supplementary Figure S8), MLD and δ (Supplementary Figure S9), kinematic viscosity
261 and δ (Supplementary Figure S10) and between copepod abundance and height-diameter difference
262 (Supplementary Figure S11). The correlations were tested by means of a Montecarlo test using
263 100,000 permutations (Jackson and Somers, 1989).

264

265 2.6.6. Phenology and niche

266 We estimated the optimum and amplitude (breadth) of the niche using nine ecological dimensions:
267 SST, euphotic depth, PAR, MLD, silicate phosphate and nitrate concentration, bathymetry and
268 distance to nearest coastlines. To do so, we estimated the weighted mean as a proxy for optimum
269 (X_{opt}) and the weighted standard deviation as a proxy for the amplitude (σ) (Figure 2 and
270 Supplementary Figure S12). These proxies were calculated for each ecological dimension:

271

$$272 \quad X_{opt} = \frac{\sum_{i=1}^t w_i x_i}{\sum_{i=1}^t w_i} \quad [8]$$

273

$$274 \quad \sigma = \frac{\sum_{i=1}^t w_i (x_i - x_{opt})^2}{\frac{t-1}{t} \sum_{i=1}^t w_i} \quad [9]$$

275

276 where w is the abundance of the diatom species, x the value of the environmental parameter or
277 copepod abundance and t the number of days in the climatology (for SST, euphotic depth, PAR, MLD,
278 silicate phosphate and nitrate concentration, and small/large copepod abundance) or the total
279 number of CPR samples when bathymetry or distance to nearest coastlines was used.

280

281 We examined the relationships between diatom niche optimum/amplitude, their day of maximum
282 abundance and the daily climatology for SST, euphotic depth, PAR, MLD, silicate phosphate and
283 nitrate concentration (Figure 2b-h). We also investigated the relationships between diatom niche
284 optimum/amplitude and height-diameter difference (Supplementary Figure S12).

285

286 We tested the niche separation between oblates and prolates by means of a Kruskal-Wallis test
287 performed on niche optima and amplitude (Supplementary Tables S13-S14). The relationships
288 between species niche optima/amplitudes and species height-diameter difference was examined by
289 applying a Spearman rank correlation coefficient and tested with a Montecarlo test using 100,000
290 simulations (Supplementary Figure S12)(Jackson and Somers, 1989).

291

292 *2.6.7. Long-term changes in the abundance of oblates and prolates*

293 We investigated long-term monthly changes in the mean abundance of oblates and prolates
294 collected by the CPR survey between 1958 and 2017 (Figure 4a). Oblate abundance in April and
295 October and prolate abundance in August were smoothed by means of a second-order simple
296 moving average (Figure 4b-d). The relationships between species abundance (in April and October for
297 oblates and August for prolates) and the long-term changes in SST, wind and solar radiations were
298 examined by applying a Spearman rank correlation coefficient and tested with a Montecarlo test
299 using 100,000 simulations (Supplementary Table S15)(Jackson and Somers, 1989).

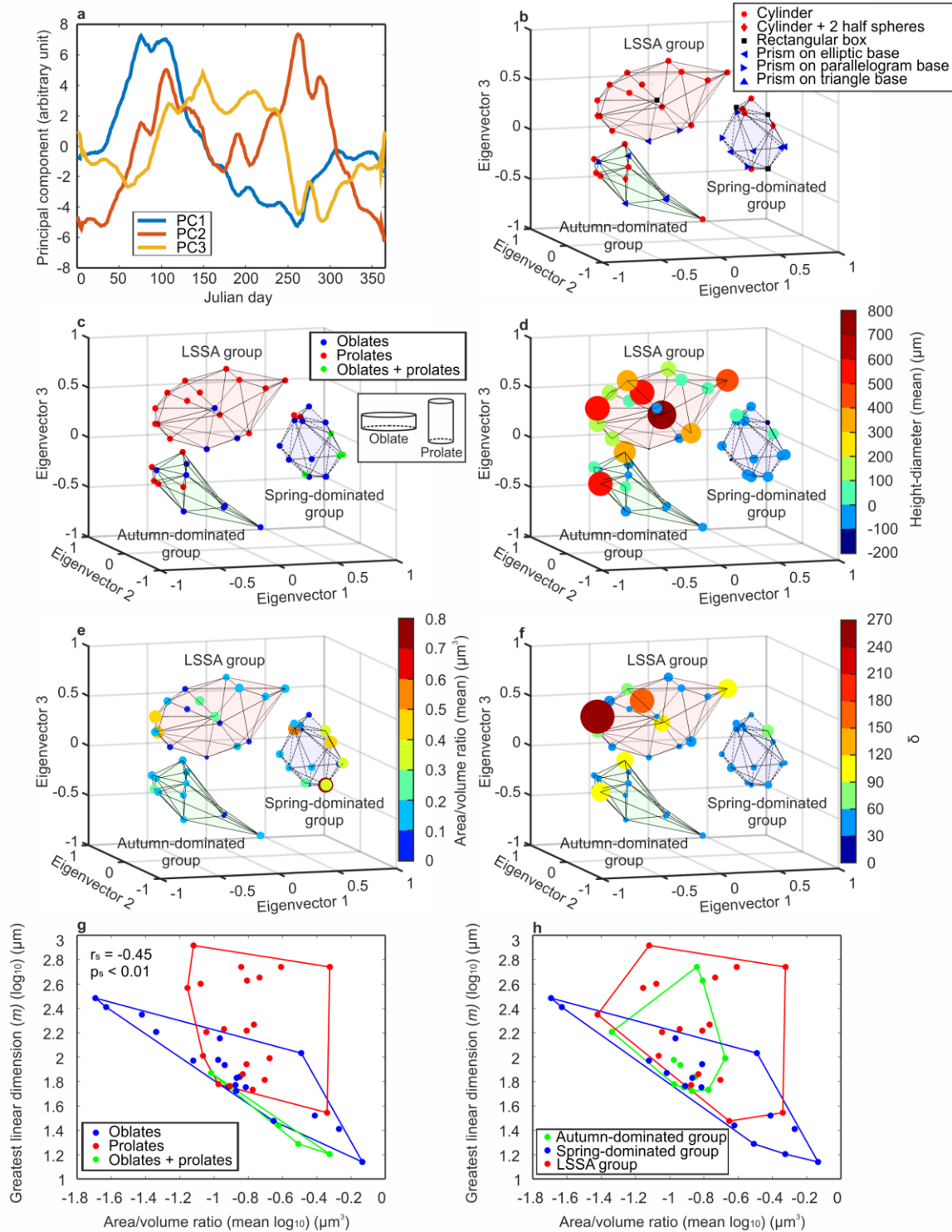
300

301 **3. Results and Discussion**

302 We first characterised ADS by means of a Principal Component Analysis (PCA) performed on a matrix
303 of daily abundance climatology (366 days) x diatom species (45 species; Methods). The abundance
304 matrix originated from data collected by the Continuous Plankton Recorder (CPR) survey between
305 1958 and 2017 in the North Sea (Supplementary Figure S1). We retained the first three Principal
306 Components (PCs), which were significant after applying a broken-stick test (Methods and

307 Supplementary Table S4). The first PC (26% of the total variance) showed a strong peak in spring at a
308 time of weak stratification and low temperature, reflecting the spring bloom, and a smaller peak in
309 late autumn at a time of decreasing temperature and stratification breakdown (Caracciolo et al.,
310 2021) (Figure 1a). The second PC (25%) exhibited a similar pattern with two peaks, the lowest in
311 spring and the highest in autumn, again reflecting both spring and autumn blooms. The third PC
312 (15%) showed high positive values from late spring to the end of summer, identifying diatoms that
313 were dominant during the stratified low-nutrients period at a time of higher zooplankton abundance
314 (Supplementary Figure S2a-c). We therefore identify three key periods in ADS, confirming a pattern
315 seen in temperate seas (Caracciolo et al., 2021; Colebrook, 1986, 1984).

316



317

318 **Figure 1. Annual Diatom Succession (ADS) and morphological traits.** (a) ADS characterized by a PCA
 319 applied on a species abundance matrix 366 days x 45 species. The first three principal components
 320 (PCs) are shown. (b-f) Relationships between the first three eigenvectors and morphological traits.
 321 Relationships between species groups and (b) morphological traits, (c) oblates and prolates, (d)
 322 height-diameter differences, (e) area/volume ratio and (f) δ . Blue area delineates the space occupied
 323 by the spring-dominated group, green area the space occupied by the autumn-dominated group and
 324 red area the space occupied by the LSSA group. (d-f) Size and colour of the bullets are scaled with (d)
 325 mean cell height-diameter difference, (e) mean area/volume ratio and (f) δ . (g-h) Relationships

326 between cell greatest linear dimension (m)(\log_{10}) and mean area/volume ratio (\log_{10}). Spearman rank
327 correlation coefficient (r_s) and its associated probability (p_s) are displayed on the top left.
328

329 We examined species phenology by studying the first three normalised eigenvectors, which
330 represent the correlation between each species and the first three PCs (Figure 1b-f). A cluster
331 analysis, performed on the first three eigenvectors, allowed us to identify three assemblages
332 (Supplementary Figures S2d-f and S4), each belonging to one of the phenological patterns we
333 identified previously (Figure 1b-f): (i) a spring-dominated group related to PC1, (ii) an autumn-
334 dominated group related to PC2 and (iii) a Late-Spring Summer Autumn (LSSA) group related to PC3
335 (Supplementary Figures S2, S4-S5).

336

337 We next studied relationships between species phenology and morphological traits. Cell shape and
338 size are major traits affecting nutrient acquisition, light capture, grazing resistance, and vertical
339 motion (Clifton et al., 2018; Karp-Boss and Boss, 2016; Litchman and Klausmeier, 2008; Naselli-Flores
340 et al., 2021; Naselli-Flores and Barone, 2011; Padisak et al., 2003). To do so, we compiled data on cell
341 size and geometrical shape from the Global Diatom Database (Leblanc et al., 2012) for 45
342 species/taxa (Methods). Spring-dominated and autumn-dominated groups comprised a mixture of
343 species of different shapes (cylindrical, rectangular box and prism) whereas the LSSA group mainly
344 comprised cylindrical diatoms (Figure 1b and Supplementary Table S1). By assuming all diatom
345 shapes to be cylindrical (note that we also performed the same analyses by assimilating diatom
346 shapes to spheroids, see below), we separated diatoms as oblates (i.e., cell diameter > cell height,
347 flattened cell) and prolates (cell diameter < cell height, elongated cell). We identified 20 oblates and
348 21 prolates, the remaining being identified as oblates/prolates (i.e. species/taxa that can be both
349 during their life cycle; Methods and Supplementary Table S2). The spring- and autumn-dominated
350 groups mainly comprised oblates (62.5% and 58% in the spring- and autumn-dominated group,
351 respectively; Figure 1c and Supplementary Table S1) and the LSSA group mostly comprised prolates
352 (82%; Figure 1c and Supplementary Table S1).

353

354 Following this result, we investigated the variations of the mean cell height-diameter difference
355 between groups more deeply (Figure 1d). Highest and lowest positive differences characterized the
356 LSSA group and the spring-dominated group, respectively. Values were more variable from the
357 autumn-dominated group. A Kruskal-Wallis test revealed significant differences and post-hoc tests
358 showed that differences occurred between LSSA and spring/autumn-dominated groups, but not
359 between spring- and autumn-dominated groups (Supplementary Table S6). Interestingly, negative
360 differences (shown in blue on the colour bar) were smaller than positive ones (from green to red;
361 Figure 1d), suggesting that cell height rather than diameter is modified during ADS; this result is
362 confirmed by insignificant differences in cell diameter and significant differences in cell height among
363 groups (Supplementary Figure S6 and Supplementary Tables S7-S8). Previous studies have suggested
364 that the size of phytoplankton is rarely greater than 300 μm (Naselli-Flores and Barone, 2011)
365 because of fundamental structural constraints imposed by natural selection, i.e. limited minimum
366 thickness and maximum diameter. For example, to avoid turbulence-induced damage and to benefit
367 from the viscosity of water, planktonic cells have to remain smaller than the Kolmogorov scale (i.e.
368 micro eddies) (Naselli-Flores et al., 2021; Reynolds, 1998) and the area/volume ratio needs to remain
369 relatively low to ensure chemical exchanges between the cell and its environment (Raven et al.,
370 2005).

371

372 Phytoplankton exhibit different cell shapes that modify their area/volume ratio to optimize nutrient
373 exchange and buoyancy with their surrounding environment (Karp-Boss and Boss, 2016; Pahlow et
374 al., 1997). Energy flux occurs through the cell surface while metabolism is related to the cell volume,
375 which explains why the ratio between surface area and volume should be high, although the building
376 of a large surface has also a negative metabolic cost (Brown et al., 2004). We did not find any
377 significant seasonal changes in the ratio between surface area and volume amongst our three groups
378 (Figure 1e and Supplementary Table S9). Similar results have been documented in tropical lakes and

379 coastal marine waters where the area/volume ratio was preserved through morphological changes
380 (Lewis, 1976; Stanca et al., 2013). We tested whether elongation (i.e. an increase in the maximum
381 linear dimension or m) could be a more relevant parameter. To do so, we used an index of cell
382 morphology δ (i.e. m times the area/volume ratio; Methods)(Naselli-Flores et al., 2021). In contrast
383 to the area/volume ratio (Figure 1e), we found significant differences in cell morphology (δ) among
384 the three groups (Figure 1f and Supplementary Table S10). Assimilating diatom shapes to spheroids
385 led to similar conclusions (Supplementary Figure S7 and Tables S11-S12). A closer look on m versus
386 sv^{-1} allowed a better understanding of why there was no significant change in the area/volume
387 ratio (Figure 1g-h). The two figures suggest that the dominance of prolates in the LSSA group during
388 the stratified low-nutrients period does not affect the area/volume ratio in contrast to oblates where
389 changes in size do influence the area/volume ratio. These results suggest that cell elongation is a way
390 of altering shape without changing the area/volume ratio that would otherwise affect nutrient
391 exchange (Karp-Boss and Boss, 2016; Pahlow et al., 1997).

392

393 Further, we examined whether phylogeny (from family to subclass level) was responsible for the
394 observed differences in traits. We found no evidence for a phylogenetic effect at the family, order
395 and superorder levels. This was not so at the subclass level; although the LSSA and autumn-
396 dominated groups were mainly composed of *Coscinodiscophycidae*, the spring-dominated group was
397 characterized by a diversity of subclasses (Supplementary Figure S3 and Table S3). This analysis,
398 therefore, shows that differences in morphological traits are also influenced by phylogeny. Other
399 studies have suggested that major morphological traits that drive strategies in nutrient uptake are
400 conserved over evolutionary time at a high phylogenetic level, a phenomenon known as trait
401 conservatism (Litchman et al., 2007). **Trait conservatism results from stabilizing selection and niche**
402 **conservatism, i.e. species keeping the shape of their niche unaltered over time because of their**
403 **propensity to remain in places** where the environment is **highly suitable for them** (Ackerly, 2003).

404 (Not all phytoplankton traits exhibit the same level of conservatism, some being more labile than
405 others. (Litchman et al., 2010; Schwaderer et al., 2011)).

406

407 Three other hypotheses could also explain the morphological changes we observed: (i) light capture
408 optimization (Naselli-Flores and Barone, 2011), (ii) buoyancy (Naselli-Flores et al., 2021; Naselli-Flores
409 and Barone, 2011; Padisak et al., 2003) and (iii) response to predation (Smetacek, 2001). We
410 investigated relationships between maximum area of light interception normalized by volume (β) and
411 Photosynthetically Active Radiation (PAR) (Methods, Supplementary Figure S8). We found no clear
412 relationship between PAR and β . Noticeably, β diminished when maximum PAR increased, which is in
413 agreement with physiology (Reynolds, 1989). However, small values of β were observed for a large
414 range of PARs, which suggests that changes in β are not modulated by PAR for most species
415 considered here. We acknowledge that physiological processes by which the cell can adapt to
416 different light intensity are complex, however (e.g. photosynthetic pigments, see Supplementary Text
417 S3)(Reynolds, 1989).

418

419 Many other studies have provided evidence that variations in cell shape might result from an
420 adaptation to turbulence through a modification in sinking velocity (Clifton et al., 2018; Margalef,
421 1978; Naselli-Flores et al., 2021; Naselli-Flores and Barone, 2011; Padisak et al., 2003). We tested this
422 hypothesis by investigating the relationship between Mixed Layer Depth (MLD, used as a proxy for
423 wind-induced turbulence intensity) and δ (Supplementary Figure S9, Methods). This analysis revealed
424 a negative relationship between maximum MLD values and δ . While oblates were found for a large
425 range of MLDs, prolates dominated low-turbulence waters. We therefore concluded that diatom
426 elongation observed during ADS may result mainly from an adaptation to buoyancy, although
427 resource acquisition and predation probably also play a role (Karp-Boss and Boss, 2016; Pahlow et al.,
428 1997; Sommer, 1998).

429

430 Studies have also found negative relationships between temperature and phytoplankton sinking
431 velocity through an alteration in viscosity (Smayda, 1970; Sournia, 1982). From Stokes' equation, and
432 considering a cell of 20 μm of diameter, sinking velocity increases of 4% for each increase of 1°C
433 because of a decrease in viscosity (Smayda, 1970). However, sinking velocity depends on cell shapes
434 (Padisak et al., 2003; Smayda, 1970; Sournia, 1982). We therefore tested the relationship between
435 kinematic viscosity and δ and found a weak but significant negative relationship (Supplementary
436 Figure S10; Methods). This result suggests that prolates may also occur in stratified warm waters
437 because their shapes slow down sinking velocity (Padisak et al., 2003). We acknowledge that we have
438 not considered all processes that can impact phytoplankton buoyancy. First, many species produce
439 organic substances that increase the viscosity of the surrounding environment and that may then
440 trigger cell aggregation, sometimes associated with minerals and particles, which may ultimately
441 increase sinking velocity (Smayda, 1970; Smetacek, 1985). Second, phytoplankton cells can also
442 develop protuberances such as spines and setae that directly increase the frictional drag or help turn
443 the longest cell dimension perpendicular to the settling axis (Padisak et al., 2003; Smayda, 1970).
444 Third, some species form chains that may affect sinking speed, although contrasting results have
445 been observed for different species with either an increase or a decrease in buoyancy (Padisak et al.,
446 2003; Smayda, 1970). Lastly, we have not considered intra-specific variations in size and seasonal
447 morphological plasticity, which can be important in many species (Ligowski et al., 2012).

448

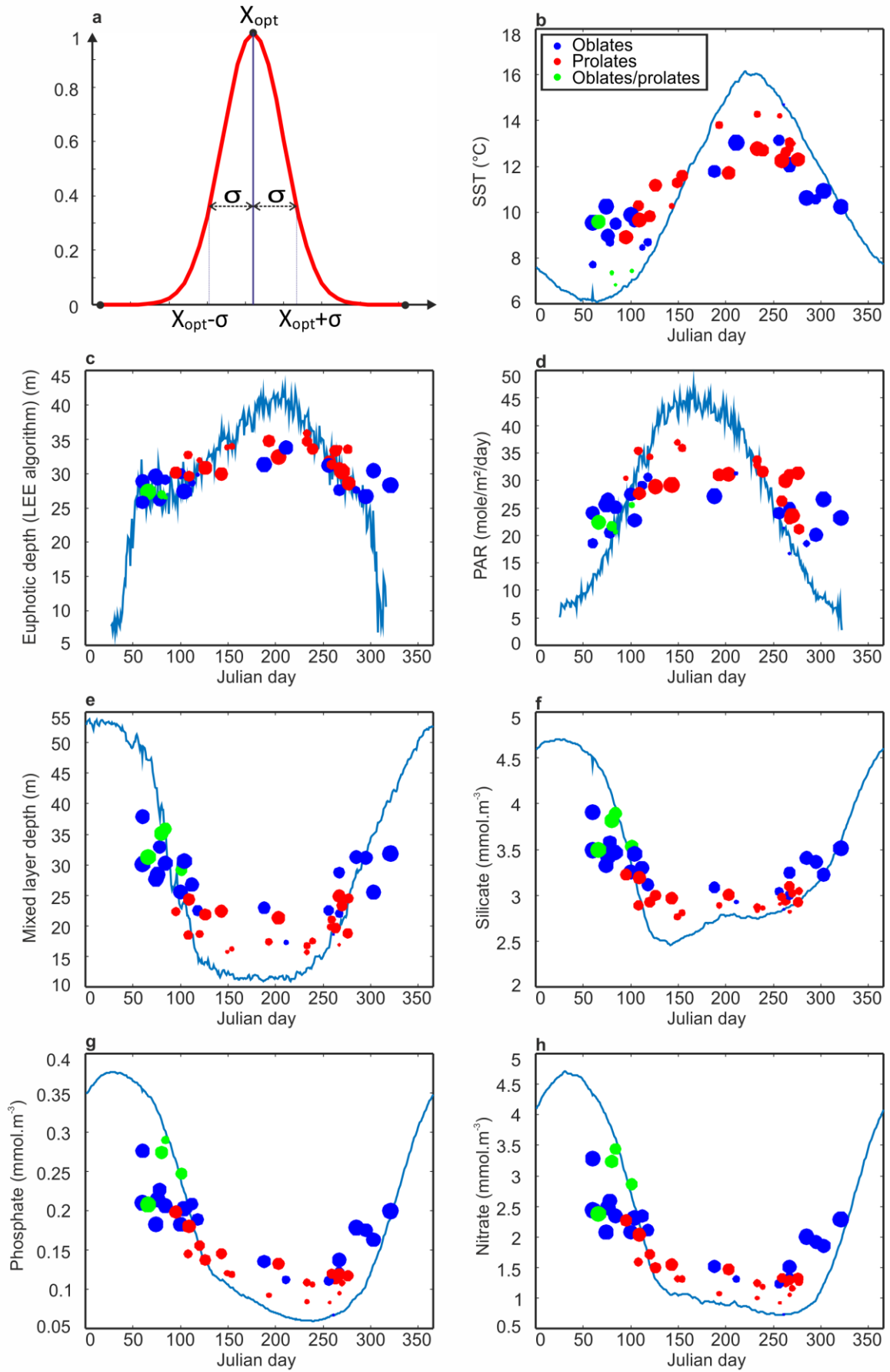
449 Lastly, we investigated whether there is a relationship between diatom shape and predation. We
450 examined the relationship between the abundance of small ($\leq 2\text{mm}$)/large ($> 2\text{mm}$) copepods and
451 morphological shape (Methods, Supplementary Figure S11). Although correlation cannot imply
452 causation, we found a nonlinear positive correlation between zooplankton abundance for small and
453 large copepods and height-diameter difference. This result is in agreement with works that have
454 suggested that changes in diatom shape may be influenced by zooplankton predation (Karp-Boss and
455 Boss, 2016; Naselli-Flores and Barone, 2011; Smetacek, 2001), although other works have shown that

456 elongated cells can be ingested by copepods when turbulence is low (Visser and Jonsson, 2000). We
457 caution that defence mechanisms in diatoms are diverse, ranging from physiological (allelopathy) to
458 phenomena such as colony formation and escape response (Pančić and Kjørboe, 2018) and that all
459 mechanisms involved could not be realistically tested in this study.

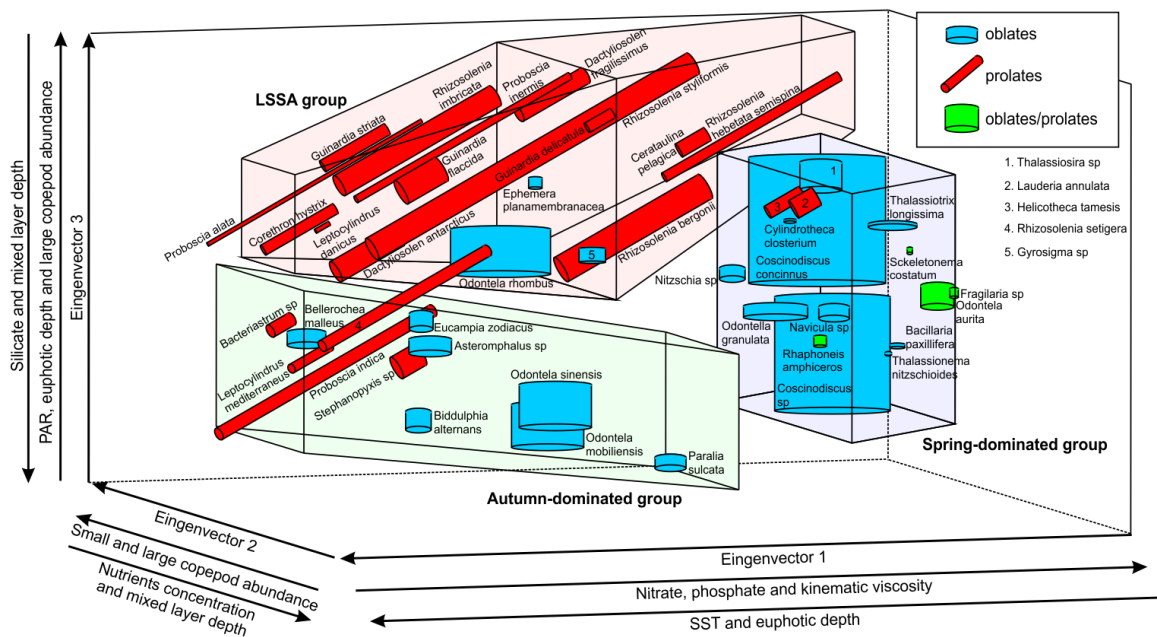
460

461 Recent works have suggested that annual plankton succession results from the niche-environment
462 interaction (Caracciolo et al., 2021). We therefore explored the relationships between cell shape and
463 ecological niche for the 45 species/taxa. Here, the ecological niche was characterised by its optimum
464 and amplitude (i.e. niche breadth) (Hutchinson, 1957); these niche parameters were assessed for
465 each species/taxa and nine environmental parameters (Methods; Figure 2a). Our results suggest that
466 morphological traits influence species' niche of diatoms and that oblates and prolates had significant
467 differences in ecological optima for all niche dimensions. Amplitudes were also distinct for four niche
468 dimensions: nutrients (nitrate, phosphate and silicate) and MLD (Figure 2b-h, Supplementary Tables
469 S13-S14). Although the relationship was less obvious for sea surface temperature and euphotic depth
470 (Figure 2b-c), optima and amplitudes plotted against daily climatology of each parameter showed a
471 clear dominance of prolates during low-nutrients, turbulence and PAR conditions (Figure 2d-h). In
472 addition, oblates were significantly more euryoecious (i.e. larger niche amplitude) than prolates with
473 respect to nutrients and MLD (Figure 2e-h, Supplementary Figure S12 and Table S14). Prolates are
474 therefore K-strategists (i.e. equilibrium species), adapted to stable environment (i.e. predictable
475 environment with low perturbations) with respect to nutrients, turbulence and stratification (low
476 MLD) whereas oblates are more r-strategists (i.e. opportunist species), adapted to a more unstable
477 environment (i.e. unpredictable) (Southwood et al., 1974). In other words, prolates (K-strategist)
478 thrive in stratified water with low turbulence and constant low-nutrient concentration whereas
479 oblates (r-strategists) thrive in turbulent waters in the absence of stratification with more variable
480 levels of nutrients concentration (Figure 2). Because oblates and prolates have distinct niches, this
481 analysis demonstrates that morphological traits influence species niche and phenology. We

482 summarize the relationships between diatom morphological traits, phenology and the environment
483 in Figure 3 (see also Supplementary Table S5).
484



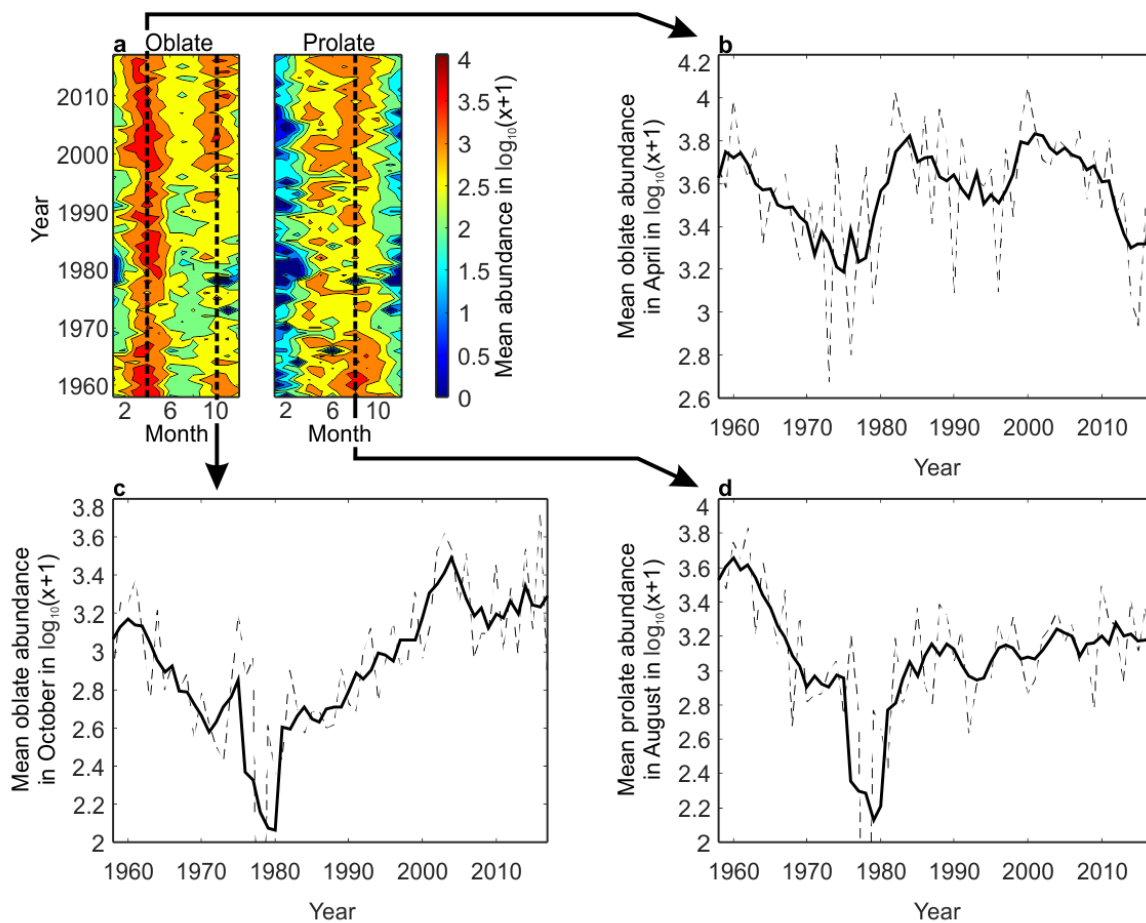
486 **Figure 2. Relationships between day of maximum abundance and ecological optima/amplitude of**
 487 **each diatom and environmental parameter.** (a) Theoretical ecological niche with X_{opt} representing
 488 species niche optimum and σ denoting niche amplitude assessed by the weighted standard deviation.
 489 The Y axis corresponds to the species abundance and the X axis to an hypothetical environmental
 490 parameter. Relationships between day of maximum abundance and niche optimum/amplitude for
 491 (b) SST, (c) euphotic depth, (d) PAR, (e) mixed layer depth (MLD), (f) silicate, (g) phosphate and (h)
 492 nitrate concentration. Blue lines correspond to the North Sea daily climatology of the parameter
 493 considered in the panel. The niche optimum can be read on the ordinate axis. The size of the bullet
 494 is a function of species' rank of the weighted standard deviation; larger bullets are associated with
 495 larger niche amplitude and therefore ranks. Oblates are in blue, prolates in red and oblates/prolates
 496 in green.



498 **Figure 3. Summary of the relationships between the first three eigenvectors, diatom shapes and**
 499 **the environment.** Cell shapes are represented by cylinders scaled with species height and diameter
 500 (Supplementary Table S2). Oblates are in blue, prolates in red and oblates/prolates in green. Species
 501 names are those recorded in the CPR dataset. Blue area delineates the space occupied by the spring-
 502 dominated group, green area the space occupied by the autumn-dominated group and red area the
 503 space occupied by the LSSA group. Correlation between the first three principal components and the
 504 environmental parameters are displayed in Supplementary Table S5. More information on the
 505 principal components can be found in Figure 1a.
 506
 507

508 Finally, we investigated long-term monthly changes in the abundance of oblates and prolates
 509 between 1958 and 2017. Our results show that both groups exhibit distinct patterns of temporal
 510 changes (Figure 4a), with oblates having a constant and high level of abundance in April (Figure 4b)
 511 but a more variable abundance in October with blooms of decreasing intensity during the 1960s and
 512 1970s, followed by a strong increase after *circa* 1980 (Figure 4c). Similar patterns are also observed

513 for prolates in August but with an abundance level below the maximum reached in 1960 (Figure 4d).
 514 The period of low abundance found for oblates and prolates between 1978 and 1982 was probably
 515 the consequence of a cold hydro-meteorological anomaly observed in the North Sea (Edwards et al.,
 516 2002). We subsequently investigated whether these long-term changes in abundance were
 517 correlated with long-term changes in Sea Surface Temperature (SST), wind and solar radiations
 518 (Supplementary Table S15). We found a nonlinear positive correlation between oblate abundance in
 519 October and SST and a negative correlation with eastward wind as well as wind intensity. A negative
 520 correlation was also found between oblate abundance in April and eastward wind. No significant
 521 correlations with northward wind and solar radiations were found. In the Northeast Atlantic region,
 522 long-term changes in SST/wind variations have led to a marked increase in diatoms, associated with a
 523 diminution in dinoflagellates (Hinder et al., 2012).
 524



525

526 **Figure 4. Long-term changes in oblate and prolate abundance (i.e. number per CPR sample)**
527 **between 1958 and 2017.** (a) Long-term monthly changes in total oblate and prolate abundance.
528 Dashed lines highlight the months that were considered in the examination of long-term changes in
529 oblates or prolates on panels (b), (c) and (d). (b-d) Long-term changes in the abundance of oblates in
530 (b) April and (c) October and (d) of prolates in August. Dashed lines represent the long-term changes
531 in diatom abundance from panel (a) and black bold lines show the smoothed long-term changes after
532 applying a second-order simple moving average. Note that the exceptional nil abundance value
533 observed for oblates and prolates in 1978 is below the y axis in the panels c and d.
534

535 Because oblates and prolates exhibit specific long-term changes, our results suggest they may
536 respond to different environmental forcing. However, it is widely assumed that diatom contribution
537 to primary production and carbon export will decline in the mid and low latitudes because ocean
538 warming will increase stratification and decrease nutrients supply to the surface ocean (Bopp et al.,
539 2013, 2005; Dutkiewicz et al., 2013; Fu et al., 2016). Such predictions are made because of an
540 oversimplification of Margalef's mandala (Margalef, 1978) assimilating diatoms to a single Plankton
541 Functional Type (PFT) that thrives when nutrients and turbulence are high (Fu et al., 2016; Kemp and
542 Villareal, 2018; Tréguer et al., 2018). Therefore, current state-of-the-art biogeochemical models only
543 consider oblates in their simulations and not prolates, but our results clearly show that diatoms,
544 through morphological adaptations, are able to exploit a wider range of environment, which is also
545 confirmed by (i) a *Tara* Oceans expedition study that has found comparable diatom diversity in
546 oligotrophic and coastal regions (Malviya et al., 2016) and by (ii) fossil records of the Mediterranean
547 sea, where sapropels (one of the most carbon-rich sediments) formation is associated with highly
548 stratified conditions and high diatom production and export (Kemp and Villareal, 2013). Hence, we
549 suggest that biogeochemical and earth-system models should consider diatom morphology by
550 defining two PFTs (i.e. oblates and prolates) in their settings to improve their predictions on the
551 consequences of climate change on primary production and carbon export.

552

553 **4. Conclusions**

554 By characterizing ADS in the North Sea with a trait-based approach, we have shown that this
555 phenomenon is controlled by the niche-environment interaction that results from seasonal changes

556 in morphological traits. Although four different hypotheses have been proposed to explain changes
557 in cell shapes (Karp-Boss and Boss, 2016; Litchman and Klausmeier, 2008; Naselli-Flores et al., 2021;
558 Naselli-Flores and Barone, 2011; Smetacek, 2001), our results suggest that cell adaptation to
559 turbulence and viscosity is of primary importance. Cell elongation gives a competitive advantage to
560 diatoms in low-turbulence and low-viscous waters because it diminishes sinking velocity (Padisak et
561 al., 2003). Our results have also shown that elongation does not affect surface/volume ratio and
562 therefore the ability of cells to absorb nutrients (Figure 1g-h). We did not find any evidence that
563 elongation might enhance light capture despite some suggestions that it might (Naselli-Flores and
564 Barone, 2011). Finally, although some studies have suggested that zooplankton can feed on large
565 chains and elongated cells (Djeghri et al., 2018; Visser and Jonsson, 2000), the positive correlation
566 between copepod abundance and elongation that we found suggests predation may also be an
567 important selective agent. Our study suggests that prolates and oblates are key adaptations to
568 specific environments, conferring to species a specific niche. The resulting niche-environment
569 interaction explains phenology and therefore the precise position of a species in the sequence of
570 ADS. Understanding the relationships between morphological traits and species niche can help us to
571 better anticipate community shifts and their functional implications for the ecosystems in the
572 context of global climate change (Litchman et al., 2012). To conclude, as both oblates and prolates
573 exhibit different long-term changes in abundance, suggesting that they might also have different
574 responses to climate forcing, we encourage biogeochemical and earth-system modelers to
575 implement these two diatom groups to improve the assessment of marine primary production and
576 carbon export.

577

578 **Acknowledgements:** We would like to thank the owners and crews that have towed the CPRs on a
579 voluntary basis for over 80 years contributing to one of the world's largest and longest ongoing
580 ecological experiments. Without these early pioneers of citizen science and broad-scale volunteer
581 monitoring projects this unique ecological dataset would never have been financially or logistically

582 viable. The authors also want to thanks Eric Lecuyer, Dimitra-Ioli Skouroliakou, Monica Michel-
583 Rodriguez and Lucie Courcot for their helpful comments during the design of this study.

584

585 **Data sharing statement:** Data used in the production of this manuscript are already freely available
586 (see Materials and Methods section and Supplementary Text S2).

587

588 **Funding information:** This work is supported by the Centre National de la Recherche Scientifique
589 (CNRS), the Region Hauts-de-France and the Marine Biological Association of the UK.

590

591 References

- 592 Ackerly, D.D., 2003. Community Assembly, Niche Conservatism, and Adaptive Evolution in Changing
593 Environments. *Int. J. Plant Sci.* 164, S165–S184. <https://doi.org/10.1086/368401>
- 594 Beaugrand, G., Brander, K.M., Lindley, J.A., Souissi, S., Reid, P.C., 2003a. Plankton effect on cod
595 recruitment in the North Sea. *Nature* 426, 661–664. <https://doi.org/10.1038/nature02164>
- 596 Beaugrand, G., Ibañez, F., Lindley, J.A., 2003b. An overview of statistical methods applied to CPR
597 data. *Prog. Oceanogr.* 58, 235–262. <https://doi.org/10.1016/j.pocean.2003.08.006>
- 598 Behrenfeld, M.J., 2010. Abandoning Sverdrup’s Critical Depth Hypothesis on phytoplankton blooms.
599 *Ecology* 91, 977–989. <https://doi.org/10.1890/09-1207.1>
- 600 Bopp, L., Aumont, O., Cadule, P., Alvain, S., Gehlen, M., 2005. Response of diatoms distribution to
601 global warming and potential implications: A global model study. *Geophys. Res. Lett.* 32.
602 <https://doi.org/10.1029/2005GL023653>
- 603 Bopp, L., Resplandy, L., Orr, J.C., Doney, S.C., Dunne, J.P., Gehlen, M., Halloran, P., Heinze, C., Ilyina,
604 T., Séférian, R., Tjiputra, J., Vichi, M., 2013. Multiple stressors of ocean ecosystems in the
605 21st century: projections with CMIP5 models. *Biogeosciences* 10, 6225–6245.
606 <https://doi.org/10.5194/bg-10-6225-2013>
- 607 Brown, J.H., Gillooly, J.F., Allen, A.P., Savage, V.M., West, G.B., 2004. Toward a metabolic theory of
608 ecology. *Ecology* 85, 1771–1789. <https://doi.org/10.1890/03-9000>
- 609 Caracciolo, M., Beaugrand, G., Hélaouët, P., Gevaert, F., Edwards, M., Lizon, F., Kléparski, L.,
610 Goberville, E., 2021. Annual phytoplankton succession results from niche-environment
611 interaction. *J. Plankton Res.* 43, 85–102. <https://doi.org/10.1093/plankt/fbaa060>
- 612 Chivers, W.J., Walne, A.W., Hays, G.C., 2017. Mismatch between marine plankton range movements
613 and the velocity of climate change. *Nat. Commun.* 8, 14434.
614 <https://doi.org/10.1038/ncomms14434>
- 615 Clifton, W., Bearon, R.N., Bees, M.A., 2018. Enhanced sedimentation of elongated plankton in simple
616 flows. *IMA J. Appl. Math.* 83, 743–766. <https://doi.org/10.1093/imamat/hxy024>
- 617 Colebrook, J.M., 1986. Environmental influences on long-term variability in marine plankton.
618 *Hydrobiologia* 142, 309–325.
- 619 Colebrook, J.M., 1984. Continuous plankton records: relationships between species of phytoplankton
620 and zooplankton in the seasonal cycle. *Marine Biology* 83, 313–323.
- 621 Cushing, D.H., 1990. Plankton Production and Year-class Strength in Fish Populations: an Update of
622 the Match/Mismatch Hypothesis. *Adv. Mar. Biol.* 26, 249–293.
623 [https://doi.org/10.1016/S0065-2881\(08\)60202-3](https://doi.org/10.1016/S0065-2881(08)60202-3)

624 Djeghri, N., Atkinson, A., Fileman, E.S., Harmer, R.A., Widdicombe, C., McEvoy, A.J., Cornwell, L.,
625 Mayor, D.J., 2018. High prey-predator size ratios and unselective feeding in copepods: A
626 seasonal comparison of five species with contrasting feeding modes. *Prog. Oceanogr.* 165,
627 63–74. <https://doi.org/10.1016/j.pocean.2018.04.013>

628 Dutkiewicz, S., Scott, J.R., Follows, M.J., 2013. Winners and losers: Ecological and biogeochemical
629 changes in a warming ocean. *Glob. Biogeochem. Cycles* 27, 463–477.
630 <https://doi.org/10.1002/gbc.20042>

631 Edwards, M., Beaugrand, G., Reid, P.C., Rowden, A.A., Jones, M.B., 2002. Ocean climate anomalies
632 and the ecology of the North Sea. *Mar. Ecol. Prog. Ser.* 239, 1–10.
633 <https://doi.org/10.3354/meps239001>

634 Edwards, M., Richardson, A.J., 2004. Impact of climate change on marine pelagic phenology and
635 trophic mismatch. *Nature* 430, 881–884. <https://doi.org/10.1038/nature02808>

636 Falkowski, P.G., Katz, M.E., Knoll, A.H., Quigg, A., Raven, J.A., Schofield, O., Taylor, F.J.R., 2004. The
637 Evolution of Modern Eukaryotic Phytoplankton. *Science* 305, 8.

638 Fu, W., Randerson, J.T., Moore, J.K., 2016. Climate change impacts on net primary production (NPP)
639 and export production (EP) regulated by increasing stratification and phytoplankton
640 community structure in the CMIP5 models. *Biogeosciences* 13, 5151–5170.
641 <https://doi.org/10.5194/bg-13-5151-2016>

642 Hinder, S.L., Hays, G.C., Edwards, M., Roberts, E.C., Walne, A.W., Gravenor, M.B., 2012. Changes in
643 marine dinoflagellate and diatom abundance under climate change. *Nat. Clim. Change* 2,
644 271–275. <https://doi.org/10.1038/nclimate1388>

645 Hutchinson, G.E., 1957. Concluding remarks. *Cold Spring Harb. Symp. Quant. Biol.* 22, 415–427.

646 Jackson, D.A., Somers, K.M., 1989. Are probability estimates from the permutation model of Mantel's
647 test stable? *Can. J. Zool.* 67, 766–769. <https://doi.org/10.1139/z89-108>

648 Jin, X., Gruber, N., Dunne, J.P., Sarmiento, J.L., Armstrong, R.A., 2006. Diagnosing the contribution of
649 phytoplankton functional groups to the production and export of particulate organic carbon,
650 CaCO₃, and opal from global nutrient and alkalinity distributions. *Glob. Biogeochem. Cycles*
651 20. <https://doi.org/10.1029/2005GB002532>

652 Jonas, T.D., Walne, A.W., Beaugrand, G., Gregory, L., Hays, G.C., 2004. The volume of water filtered
653 by a Continuous Plankton Recorder sample: the effect of ship speed. *J. Plankton Res.* 26,
654 1499–1506. <https://doi.org/10.1093/plankt/fbh137>

655 Karp-Boss, L., Boss, E., 2016. The Elongated, the Squat and the Spherical: Selective Pressures for
656 Phytoplankton Shape, in: Glibert, P.M., Kana, T.M. (Eds.), *Aquatic Microbial Ecology and
657 Biogeochemistry: A Dual Perspective*. Springer International Publishing, Cham, pp. 25–34.
658 https://doi.org/10.1007/978-3-319-30259-1_3

659 Katz, M.E., Wright, J.D., Miller, K.G., Cramer, B.S., Fennel, K., Falkowski, P.G., 2005. Biological
660 overprint of the geological carbon cycle. *Mar. Geol.* 217, 323–338.

661 Kemp, A.E.S., Villareal, T.A., 2018. The case of the diatoms and the muddled mandalas: Time to
662 recognize diatom adaptations to stratified waters. *Prog. Oceanogr.* 167, 138–149.
663 <https://doi.org/10.1016/j.pocean.2018.08.002>

664 Kemp, A.E.S., Villareal, T.A., 2013. High diatom production and export in stratified waters – A
665 potential negative feedback to global warming. *Prog. Oceanogr.* 119, 4–23.
666 <https://doi.org/10.1016/j.pocean.2013.06.004>

667 Leblanc, K., Arístegui, J., Armand, L., Assmy, P., Beker, B., Bode, A., Breton, E., Cornet, V., Gibson, J.,
668 Gosselin, M.-P., Kopczynska, E., Marshall, H., Peloquin, J., Piontkovski, S., Poulton, A.J.,
669 Quéguiner, B., Schiebel, R., Shipe, R., Stefels, J., van Leeuwe, M.A., Varela, M., Widdicombe,
670 C., Yallop, M., 2012. A global diatom database – abundance, biovolume and biomass in the
671 world ocean. *Earth Syst. Sci. Data* 4, 149–165. <https://doi.org/10.5194/essd-4-149-2012>

672 Legendre, P., Legendre, L., 1998. *Numerical Ecology*. Elsevier, Amsterdam - Lausanne - New York -
673 Oxford - Shannon - Singapore - Tokyo.

674 Lewis, W.M., 1976. Surface/Volume Ratio: Implications for Phytoplankton Morphology. *Science* 192,
675 885–887. <https://doi.org/10.1126/science.192.4242.885>

676 Ligowski, R., Jordan, R.W., Assmy, P., 2012. Morphological adaptation of a planktonic diatom to
677 growth in Antarctic sea ice. *Mar Biol* 11.

678 Litchman, E., de Tezanos Pinto, P., Klausmeier, C.A., Thomas, M.K., Yoshiyama, K., 2010. Linking traits
679 to species diversity and community structure in phytoplankton. *Hydrobiologia* 653, 15–28.
680 <https://doi.org/10.1007/s10750-010-0341-5>

681 Litchman, E., Edwards, K.F., Klausmeier, C.A., Thomas, M.K., 2012. Phytoplankton niches, traits and
682 eco-evolutionary responses to global environmental change. *Mar Ecol Prog Ser* 470, 235–
683 248. <https://doi.org/doi:10.3354/meps09912>

684 Litchman, E., Klausmeier, C.A., 2008. Trait-Based Community Ecology of Phytoplankton. *Annu. Rev.*
685 *Ecol. Evol. Syst.* 39, 615–639. <https://doi.org/10.1146/annurev.ecolsys.39.110707.173549>

686 Litchman, E., Klausmeier, C.A., Schofield, O.M., Falkowski, P.G., 2007. The role of functional traits and
687 trade-offs in structuring phytoplankton communities: scaling from cellular to ecosystem
688 level. *Ecol. Lett.* 10, 1170–1181. <https://doi.org/10.1111/j.1461-0248.2007.01117.x>

689 Malviya, S., Scalco, E., Audic, S., Vincent, F., Veluchamy, A., Poulain, J., Wincker, P., Iudicone, D., de
690 Vargas, C., Bittner, L., Zingone, A., Bowler, C., 2016. Insights into global diatom distribution
691 and diversity in the world’s ocean. *Proc. Natl. Acad. Sci.* 113, 1516–1525.
692 <https://doi.org/10.1073/pnas.1509523113>

693 Margalef, R., 1978. Life-forms of phytoplankton as survival alternatives in an unstable environment.
694 *Oceanol. Acta* 1, 493–509.

695 Naselli-Flores, L., Barone, R., 2011. Invited Review - Fight on Plankton! or, Phytoplankton Shape and
696 Size as Adaptive Tools to Get Ahead in the Struggle for Life. *Cryptogam. Algal.* 32, 157–204.
697 <https://doi.org/10.7872/crya.v32.iss2.2011.157>

698 Naselli-Flores, L., Zohary, T., Padišák, J., 2021. Life in suspension and its impact on phytoplankton
699 morphology: an homage to Colin S. Reynolds. *Hydrobiologia* 848, 7–30.
700 <https://doi.org/10.1007/s10750-020-04217-x>

701 Nelson, D.M., Tréguer, P., Brzezinski, M.A., Leynaert, A., Quéguiner, B., 1995. Production and
702 dissolution of biogenic silica in the ocean: Revised global estimates, comparison with regional
703 data and relationship to biogenic sedimentation. *Glob. Biogeochem. Cycles* 9, 359–372.
704 <https://doi.org/10.1029/95GB01070>

705 Padišák, J., Soroczki-Pinter, E., Reznér, Z., 2003. Sinking properties of some phytoplankton shapes and
706 the relation of form resistance to morphological diversity of plankton – an experimental
707 study. *Hydrobiologia* 500, 243–257.

708 Pahlow, M., Riebesell, U., Wolf-Gladrow, D.A., 1997. Impact of cell shape and chain formation on
709 nutrient acquisition by marine diatoms. *Limnol. Oceanogr.* 42, 1660–1672.
710 <https://doi.org/10.4319/lo.1997.42.8.1660>

711 Pančić, M., Kiørboe, T., 2018. Phytoplankton defence mechanisms: traits and trade-offs: Defensive
712 traits and trade-offs. *Biol. Rev.* 93, 1269–1303. <https://doi.org/10.1111/brv.12395>

713 Pilson, M.E.Q., 2013. *An Introduction to the Chemistry of the Sea.*, second edition. ed. Cambridge
714 University Press.

715 Platt, T., Fuentes-Yaco, C., Frank, K.T., 2003. Spring algal bloom and larval fish survival. *Nature* 423,
716 398–399.

717 Raven, P., Johnson, G., Losos, J., Singer, S., 2005. *Biology.* Mc Graw-Hill.

718 Reid, P.C., Colebrook, J.M., Matthews, J.B.L., Aiken, J., Continuous Plankton Recorder Team, 2003.
719 The Continuous Plankton Recorder: concepts and history, from Plankton Indicator to
720 undulating recorders. *Prog. Oceanogr.* 58, 117–173.
721 <https://doi.org/10.1016/j.pocean.2003.08.002>

722 Reynolds, C.S., 1998. Plants in motion: Physical - biological interaction in the plankton, in: Imberger, J.
723 (Ed.), *Coastal and Estuarine Studies.* American Geophysical Union, Washington, D. C., pp.
724 535–560. <https://doi.org/10.1029/CE054p0535>

725 Reynolds, C.S., 1989. Physical determinants of phytoplankton succession, in: Sommer, U. (Ed.),
726 *Plankton Ecology Succession in Plankton Communities.* Springer-Verlag, Berlin, Heidelberg,
727 New York, London, Paris, Tokyo, p. 377.

728 Schwaderer, A.S., Yoshiyama, K., de Tezanos Pinto, P., Swenson, N.G., Klausmeier, C.A., Litchman, E.,
729 2011. Eco-evolutionary differences in light utilization traits and distributions of freshwater
730 phytoplankton. *Limnol. Oceanogr.* 56, 589–598. <https://doi.org/10.4319/lo.2011.56.2.0589>
731 Smayda, T., 1970. The suspension and sinking of phytoplankton in the sea. *Oceanogr. Mar. Biol. Ann.*
732 *Rev.* 8, 353–414.
733 Smetacek, V., 2001. A watery arms race. *Nature* 411, 745.
734 Smetacek, V., 1985. Role of sinking in diatom life-history cycles: ecological, evolutionary and
735 geological significance. *Mar. Biol.* 84, 239–251.
736 Sommer, U., 1998. Silicate and the functional geometry of marine phytoplankton. *J. Plankton Res.* 20,
737 1853–1859. <https://doi.org/10.1093/plankt/20.9.1853>
738 Sournia, A., 1982. Form and function in marine phytoplankton. *Biol. Rev.* 57, 347–394.
739 Southwood, T.R.E., May, R.M., Hassell, M.P., Conway, G.R., 1974. Ecological strategies and population
740 parameters. *Am. Nat.* 108, 791–804.
741 Stanca, E., Cellamare, M., Basset, A., 2013. Geometric shape as a trait to study phytoplankton
742 distributions in aquatic ecosystems. *Hydrobiologia* 701, 99–116.
743 <https://doi.org/10.1007/s10750-012-1262-2>
744 Tréguer, P., Bowler, C., Moriceau, B., Dutkiewicz, S., Gehlen, M., Aumont, O., Bittner, L., Dugdale, R.,
745 Finkel, Z., Iudicone, D., Jahn, O., Guidi, L., Lasbleiz, M., Leblanc, K., Levy, M., Pondaven, P.,
746 2018. Influence of diatom diversity on the ocean biological carbon pump. *Nat. Geosci.* 11,
747 27–37. <https://doi.org/10.1038/s41561-017-0028-x>
748 Visser, A.W., Jonsson, P.R., 2000. On the reorientation of non-spherical prey particles in a feeding
749 current. *Journal of Plankton Research* 22, 761–777.
750